Segmentation of Liver Vasculature From Contrast Enhanced CT Images Using Context-Based Voting

Yanling Chi*, Jimin Liu, Sudhakar K. Venkatesh, Su Huang, Jiayin Zhou, *Member, IEEE*, Qi Tian, *Senior Member, IEEE*, and Wieslaw L. Nowinski

***Abstract*—A novel vessel context-based voting is proposed for automatic liver vasculature segmentation in CT images. It is able to conduct full vessel segmentation and recognition of multiple vasculatures effectively. The vessel context describes context information of a voxel related to vessel properties, such as intensity, saliency, direction, and connectivity. Voxels are grouped to liver vasculatures hierarchically based on vessel context. They are first grouped locally into vessel branches with the advantage of a vessel junction measurement and then grouped globally into vasculatures, which is implemented using a multiple feature point voting mechanism. The proposed method has been evaluated on ten clinical CT datasets. Segmentation of third-order vessel trees from CT images (0.76 × 0.76 × 2.0 mm) of the portal venous phase takes less than 3 min on a PC with 2.0 GHz dual core processor and the average segmentation accuracy is up to 98%.**

***Index Terms*—Liver vasculature segmentation, multiple feature point voting, vessel context, vessel junction measure.**

I. Introduction

THE LIVER vessel segmentation is the basis of many clinical applications. For example, liver surgical planning requires accurate analysis on the structures of liver vessels and the locations of tumors related to these structures. Automatic and robust vasculature segmentation is, therefore, of great benefit in effective and efficient analysis and quantitative measure of these structures. Liver vessel segmentation in CT images is challenging due to noise. In addition, the vascular anatomy of the liver is complex [1]. There are four different tubular systems that supply and drain the liver: portal vein, hepatic vein, hepatic artery, and bile duct. Since the portal vein, the hepatic artery, and the bile ducts are parallel channels within portal tract, the portal vein and hepatic vein represent the main vessel structures inside the liver. However, the portal vein and hepatic veins show similar intensity value on CT images due to their similarity in the enhancement characteristics. They are curvy, twist, occlude one another and sometimes are seriously distorted by liver tumors. Therefore, it is difficult to segment and distinguish between them. In addition, low contrast and partial volume effect impose more difficulties upon the automatic liver vessel segmentation.

Many methods [2]–[9] are published on 3-D vessel segmentation. One can refer to [9] for a comprehensive review. For example, the probabilistic vessel axis [2] and level sets-based methods [3], [4] address cerebral vasculature segmentation. However, it is difficult to justify their performances on actual liver vessel segmentation in CT scans since they only extract one artery/vein system, and some methods are only evaluated on synthetic data or parts of CT/MR angiography of high image quality. The particle filter based [5], minimum cost path [2], [6], connected component and region grow [7], and topological method [8] are on coronary artery tracking. However, the methods cannot be generalized to liver vessel segmentation naturally. On the one hand, these tracking methods have limitations on tracking vessels across tumors. For example, user guidance [2], [6] is required when tracing through regions that contains diseased portions, kissing vessels, and thin vessels. Particle filters [5] and reconnection scheme [7] are designed to tracing a coronary artery with pathologies, but the pathologies on a coronary artery (calcification, stent, and stenosis) are quite different from a liver tumor with respect to appearance. The liver tumor is of a big size relatively to a vessel and causes a sudden change of intensity. The vessel inside the tumor might be invisible and quite difficult to predict. In [8], only a small gap due to intensity discontinuity can be filled. On the other hand, the methods cannot distinguish between different vasculatures.

There are only a few studies published on liver vasculature segmentation [10]–[12], [14]. Friman *et al*. [10] proposed a multiple hypothesis tracking method to segment the liver artery based on 3-D template matching. The method is evaluated on synthetic data and high resolution CT scans (0.8 × 0.8 × 0.6 mm). It has advantages on vessel detection under a homogeneous background. But it is ineffective when coping with touching vessels. As for other liver vasculatures, e.g., the portal vein and hepatic vein, a homogeneous background is difficult to guarantee. In the portal venous phase, the portal vein and hepatic vein are relatively big, having much visible bifurcations with respect to the artery and are entangled with one another. In addition, seed points are required to be manually set for

Manuscript received June 15, 2010; revised August 29, 2010 and November 2, 2010; accepted November 3, 2010. Date of publication November 18, 2010; date of current version July 20, 2011. This work was supported by the Agency for Science, Technology and Research, Singapore, under Grant JCOAG03_FG05_2009. *Asterisk indicates corresponding author.*

*Y. Chi is with the Biomedical Imaging Laboratory, A∗STAR, Singapore 138671 (e-mail: chi_yanling@sbic.a-star.edu.sg).

J. Liu and S. Huang are with the Biomedical Imaging Laboratory, A∗STAR, Singapore 138671 (e-mail: liujm@sbic.a-star.edu.sg; huangsu@sbic.a-star.edu.sg).

S. K. Venkatesh is with the Department of Diagnostic Imaging, National University Hospital, Singapore 119074 (e-mail: dnrskv@nus.edu.sg).

J. Zhou and Q. Tian are with the Institute for Infocomm Research, A∗STAR, Singapore 138632 (e-mail: jzhou@i2r.a-star.edu.sg; tian@i2r.a-star.edu.sg).

W. L. Nowinski is with the Biomedical Imaging Laboratory, A∗STAR, Singapore 138671, and also with the University of Washington Medical Center, Seattle, WA 98195 USA (e-mail: wieslaw@sbic.a-star.edu.sg).

Color versions of one or more of the figures in this paper are available online at http://ieeexplore.ieee.org.

Digital Object Identifier 10.1109/TBME.2010.2093523

0018-9294/$26.00 © 2010 IEEE

every tracing of branches, and the branches obtained are taken for granted a part of vasculature to segment. There is no mechanism to distinguish between different vasculatures. Thus, the algorithm's application to portal vein and hepatic vein segmentation is limited. In [11], vessels are segmented using Boykov's graph cuts algorithm driven by a 3-D geometrical moment-based detector of cylindrical shapes. The authors claimed that the portal vein and hepatic vein are naturally separated well using their method in the experiments. Thus, identification of different vessels is unnecessary. This contradicts our findings. Due to noise and the vessel course, e.g., a close distance or being parallel sometimes, discontinuity or touching vessels are almost unavoidable in CT images. These problems have to be tackled during vessel segmentation. Bauer *et al*. [12] proposed to separate and segment interwoven tubular tree structures simultaneously using a two-step method, bottom-up identifying of tubular object and top-down grouping of these objects into tree structures followed by graph cut for segmentation/evolution. In their method, the tubular object is represented as a central line whose end points are considered for grouping. The central line representation has advantage on separating overlap vessels, but extraction of central line or skeletonization is sensitive to noise and outliers [13]. Thus, grouping based on such skeleton is prone to errors. In [14], a matched filter is used to enhance vessel structures, and the genetic algorithm is applied for searching globally for the most likely vasculatures. Their method is inefficient, since its computation time is claimed of the order of one hour. Selle *et al*. [15] proposed a region-growing segmentation with automatically adjusted thresholds. The vessel separation is based on vasculatures' skeletons facilitated by the user's interaction. Their method employed only vessel intensity feature and failed to take into account the vessel structure feature. Manual corrections are required when segmentation errors occur.

In summary, most of the earlier studies segment and identify liver vasculatures using central line-based methods that are good at vessel separation but sensitive to noise and outliers [13]. These studies thus have to either make strong assumptions for effective tracking, e.g., a homogeneous background, or conduct elaborate postprocessing for desirable central line description.

Compare with the central line-based methods, the region-based methods are relatively simple but robust to noise and outliers [16]. However, few studies address liver vessel segmentation using the region-based methods. The one in [11] addressing hepatic vasculatures oversimplifies segmentation complexity by distinguishing different vessels manually or assuming there are no touching vessels. The one in [15] overlooked vessel structure feature and required the facilities from user's interaction.

In this paper, a vessel context-based voting is proposed to segment and identify liver vasculatures using region-based features. It represents vessels in terms of shape and intensity within a local region using vessel context, and segments and separates vessels hierarchically based on vessel context and its derived features. It identifies vasculatures by multiple feature points voting on optimal structures. Generally, its contributions are:

1) a novel region-based approach being able to conduct full vessel segmentation and recognition of different vasculatures in CT scans;
2) a vessel context representation that not only includes static vessel properties at the voxel, such as vessel intensity and saliency, but also indicates where the vessel should extend to in the case that vessel is discontinuous in intensity/saliency due to low contrast and noise;
3) a hierarchical mechanism to extract vasculatures, which is able to generalize the application to pathologic (tumor) volumes;
4) a multiple feature voting mechanism able to identify different vasculatures robustly;
5) a junction measurement that enables touching vessels being handled by a threshold operation.

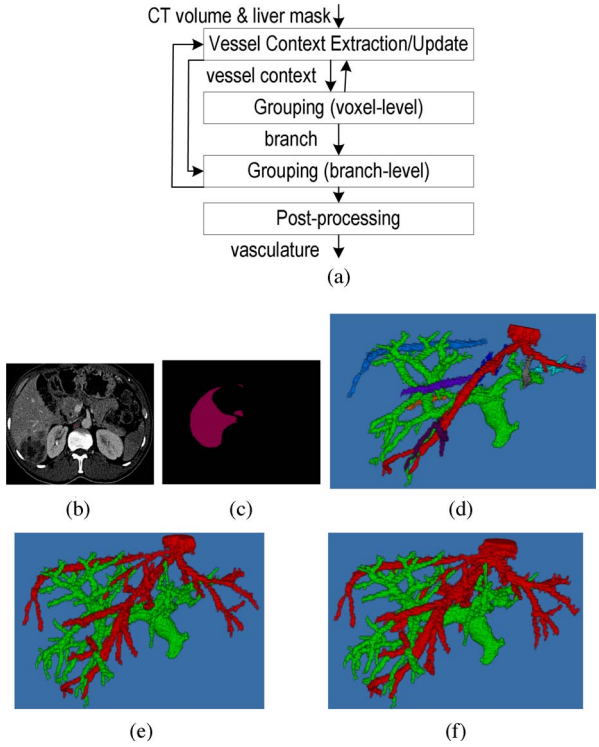

Fig. 1. Flowchart of the proposed method: (a) flowchart, (b) CT image, (c) liver mask, (d) segmented 20 branches in color, (e) segmented hepatic vein in red and portal vein in green, (f) postprocessed hepatic vein and portal vein.

II. Method

A novel approach is proposed for liver vasculature segmentation, which first extracts vessel context from input and then votes on vessel structures. Here, the liver has been delineated using MIUE [17], and the liver scan has been processed to be isotropic.

The system flowchart is shown in Fig. 1. The system input are clinical CT images of portal venous phase and the liver mask as binary images provided along with the CT images. After vessel context extraction, voxels are first locally grouped into branches based on vessel context. Then, a branch-level grouping is conducted globally by voting on vasculatures. Vessel context will be updated after each successful group operation until no fit branches are left as shown in Fig. 1(a). A postprocessing is conducted for slightly expending, smoothing, and hole-filling.

The segmented vasculatures are 3-D reconstructed for visualization. The examples of input, intermediate results, and final result are also displayed in Fig. 1(b)–(f) for clear illustration. The inputs are shown in Fig. 1(b)–(c). In Fig. 1(d), 20 example branches are displayed in color. In Fig. 1(e), the segmented portal vasculature (green) and hepatic vasculature (red) are illustrated. Fig. 1(f) shows the segmented portal (green) and hepatic vasculature (red) after postprocessing.

A. Vessel Context Extraction

Usually, in liver CT images, an expert observer marks a vessel by judging that it is on a recognizable, smooth, connected tubular structure, and that the tube is locally brighter than the background. It enlightens us to describe a voxel by its vessel context related to vessel properties, such as:

1) intensity value;
2) vessel saliency that measures the chance of a voxel coming from a tubular structure;
3) vessel direction, i.e., direction of tubular structure; and
4) connectivity of tubular structure that measures the potential paths to extend the tubular structure to another one.

Numerically, the vessel context of a voxel $p(x, y, z)$ can be represented as a quartet by

$$SC_p = \{\text{intensity, saliency, direction, connectivity}\}. \quad (1)$$

The *intensity* measures the brightness at voxel p. The *saliency* and *direction* are calculated based on the eigenvalues and eigenvectors of Hessian matrix in (2) and (3) using method described in [18]

$$\text{saliency} = \begin{cases} 0, & \text{if } \lambda_2 > 0 \text{ or } \lambda_3 > 0 \text{ or } \lambda_3/\lambda_2 < 0.5 \\ \left(1 - \exp\left(-\dfrac{R_A^2}{2\alpha^2}\right)\right) \exp\left(-\dfrac{R_B^2}{2\beta^2}\right) \left(1 - \exp\left(-\dfrac{R_C^2}{2c^2}\right)\right), & \text{others} \end{cases} \quad (2)$$

$$\text{direction} = \begin{cases} 0, & \text{saliency} = 0 \\ e_1, & \text{saliency} \neq 0 \end{cases} \quad (3)$$

where $\lambda_1, \lambda_2, \lambda_3$ $(\lambda_1 > \lambda_2 > \lambda_3)$ are eigenvalues of Hessian matrix at p, and e_1, e_2, e_3 are eigenvectors. $R_A = |\lambda_2|/|\lambda_3|$, $R_B = |\lambda_1| \Big/ \sqrt{|\lambda_2 \lambda_3|}$, $R_C = \sqrt{\sum_{j=1,2,3} \lambda_j^2}$. The α, β are fixed to 0.5 and c is set as half the value of the maximum Hessian norm, as described in [18].

$$\text{connectivity}_{(i,j)} = \begin{cases} 1, & \text{if } l \leq 1 \\ \exp\left(-\dfrac{s^2}{\sigma_1^2}\right) \exp\left(-\dfrac{k^2}{\sigma_2^2}\right), & \text{if } l > 1, -\dfrac{\pi}{2} \leq \theta \leq \dfrac{\pi}{2} \\ 0, & \text{others.} \end{cases} \quad (4)$$

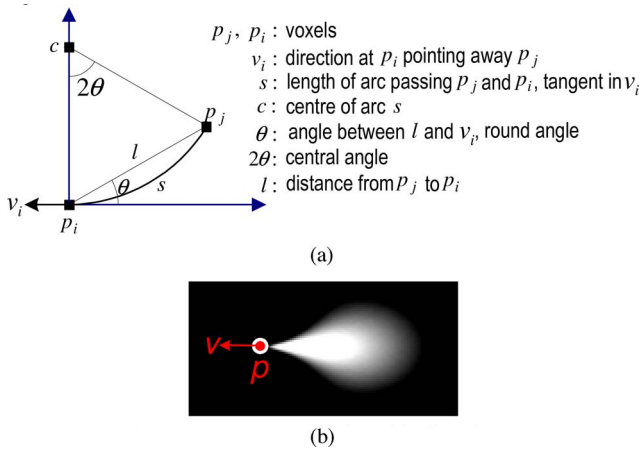

Fig. 2. Illustration of connectivity calculation. (a) Symbols used in connectivity$_{(i,j)}$ calculation. (b) Connectivity around p with direction v.

The *connectivity* measures all potential paths to extend a tubular structure of $p(x, y, z)$ to another one. For clear description, an example of one path measure is given. A potential path is defined as a smooth arcoid connection between voxel p_i on one structure and voxel p_j on another structure. The connectivity$_{(i,j)}$ is used to measure this connection regarding length and curvature. Given arc length s and curvature k, connectivity $_{(i,j)}$ is inversely proportional to s and k, and numerically calculated as in (4), where $s = \theta l / \sin\theta$, $k = 2\sin\theta/l$, and other symbols are shown in Fig. 2(a) for references. The selection of σ_1 and σ_2 will be given in Section II-C (in *Multiple feature point voting mechanism*). If $l \leq 1$, it means p_i and p_j are immediately connected. Since vessels are connected structure, the voxels immediately connected (six connections in 3-D) are give the highest connectivity$_{(i,j)}$, i.e., 1. If $l > 1$, it means p_i and p_j are not immediately connected. For voxels that are not immediately connected, the connectivity$_{(i,j)}$ decrease with the increasing of arc length s and curvature k, similar to concepts in [19]. The range of θ is from $-\pi/2$ to $\pi/2$, i.e., p_j, is in the opposite side of v_i pointing to. A special example is if p_i is an end point of a broken tube structure, there is only one direction this tubular structure can extend at p_i. The smooth arcoid connection passing p_i and p_j is on the only plane determined by p_i, v_i, and p_j. The connectivity at $p(x, y, z)$ is composed of all the connectivity$_{(i,j)}$, and is plotted in Fig. 2(b). The higher connectivity$_{(i,j)}$ value, the brighter pixel. It can be observed that the connectivity describes a possible region where a tube structure can extend into through voxel p. The shape of the region is determined by σ_1 and σ_2 in (4). If σ_1 dominates, the region will be a long and narrow one along v, i.e., it is less possible that a tubular structure extends curvedly. Otherwise, if σ_2 dominates, the region will be a short and wide one along v, i.e., it is more possible that a tubular structure will extend curvedly. The σ_1 and σ_2 can be adjusted to cater for different vessels.

B. Grouping on Voxel Level

Psychology studies indicated that a shape can be viewed as a hierarchical structure, which is formed around one or several

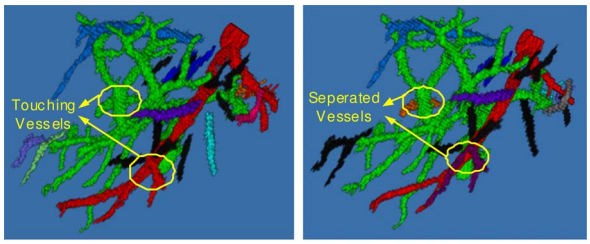

Fig. 3. Vessel branches in color after voxel-level grouping, (a) examples of touching vessels only use (6), (b) touching vessels are separated after using (7) and (8).

centers [16]. The portal vein and hepatic artery supply the liver by branching into sinusoids, while the liver sinusoids join to form the hepatic vein to drain the liver. Sinusoids are invisible on CT scans; therefore, the portal vein and hepatic vein are visually separated vasculatures. Moreover, the portal vein bifurcation is outside the liver capsule in about one half of patients [1]. These findings make it theoretically possible to extract the liver vasculatures hierarchically. The proposed mechanism extracts vasculature both locally (voxel level) and globally (branch level) based on vessel context. After vessel context extraction, voxels are first locally grouped into vessel branches based on vessel context. A branch-level grouping is then conducted globally by voting on optimal vasculatures.

In voxel-level grouping, vessel branches are regarded as clusters of voxels with similar vessel context. Given a seed point B_0 voxels with similar intensity, saliency, and immediate connections, $p_1 \dots p_i, p_{i+1} \dots p_n$, are grouped recursively to construct a branch B using (5) and (6). Seed point and similar voxel selection transverse all the volume until all voxels are processed. The threshold for *intensity* T_{int} is determined experimentally. Initially, T_{int} is set in a way so that 10% liver voxels inside the liver region have the intensities greater than T_{int}, and then it can be adjusted slightly according to image qualities

$$\text{connectivity}_{(i+1,B_i)} = \max_{j \in B_i}(\text{connectivity}_{(i+1,j)}) \tag{5}$$

$$B_{i+1} = B_i \bigcup \left\{ p_{i+1} \left| \begin{array}{l} \text{int ensity} > T_{\text{int}} \\ \text{saliency} > 0 \\ \text{connectivi } ty_{(i+1,B_i)} \geq 1 \end{array} \right. \right\}. \tag{6}$$

Vessel branches generated using (6) might be touching vessels, as illustrated in Fig. 3(a), where two or more parallel vessels (or vessels passing by) were grouped into one vessel branch due to close distance and noise. To separate these vessels, topological analysis is commonly used. However, it is undesirable since the positions of kissing vessels are unknown and global searching is inefficient. A filter that can enhance vessels and weaken adhesions is desirable. With such a filter, a simple threshold is expected to remove all the adhesions and separate kissing vessels once for all. A junction measurement is thus proposed, which measures voxel's dissimilarity to that of a junction voxel. A junction refers to the connection region of touching vessels and the junction measurement is calculated in

$$D_{\text{junction}}(p(x,y,z)) = \text{saliency} * \exp\left(-\frac{r^2}{\sigma_3^2}\right) \exp\left(-\frac{w^2}{\sigma_4^2}\right). \tag{7}$$

Voxels at a junction are featured as the relatively low *saliency* in the "central" part of a "thick" vessel. A low *saliency* means voxels at junction may not be vessels, but be diffusion of vessels or noise. The "central" part is account for the connection region of touching vessels being between them. A "thick" vessel is because touching vessel consists of multiple vessels at the junction. The *saliency* is calculated in vessel context. The $\exp(-r^2/\sigma_3^2)$ measures how much a voxel is on the "central" part in a branch, where r is from distance map of touching branches. The $\exp(-w^2/\sigma_4^2)$ measures how "thick" branch the voxel is on, where w is the scale at which saliency is obtained [18]. Given a touching branch, the $\exp(-r^2/\sigma_3^2)$ is minimized at central region, and $\exp(-w^2/\sigma_4^2)$ is minimized at regions along central axis. The reason that both are used is for self-enhancement, and this ensures good performance in case that the accuracy of r or w is inversely affected by noise. The lower value of D_{junction} at voxel $p(x,y,z)$, the higher possibility that $p(x,y,z)$ is at a junction. Thus, a threshold operation can be employed to trim branches and subtrees based on D_{junction} as

$$\text{SC}_p = \{\text{intensity}, 0, 0, \text{connectivity}\}, \text{ if } D_{\text{junction}} < T_2. \tag{8}$$

The voxels with low D_{junction} are removed from the branch. By removing the connection points, i.e., junction voxels, touching vessels will be separated. In Fig. 3(b), the separated vessels are displayed and plotted in different colors.

For a touching vessel, three items in (7) are all minimized in connection region. The threshold operation can remove misclassified voxels from the touching region. Thus, one touching vessels can be separated as two or more. For a normal vessel, since *saliency* is maximized in central region even though $\exp(-r^2/\sigma_3^2)$ and $\exp(-w^2/\sigma_4^2)$ are low, D_{junction} is still high and few voxels are removed after thresholding. For bifurcation, the *saliency* may be low in bifurcation region and so do $\exp(-r^2/\sigma_3^2)$ and $\exp(-w^2/\sigma_4^2)$. The D_{junction} is thus relatively low. It is possible to separate branches from the tree/subtree using (8). However, these branches and trees can be regrouped together in a high level with a result of unaffected final vasculature, see Section II-C. The parameters σ_3, σ_4, and T_2 are determined experimentally. The values of σ_3 and σ_4 are fixed as 10 and 5 for all datasets, while T_2 is set 0.1 for a normalized D_{junction}.

Example results of touching vessels being separated using (7) and (8) are illustrated in Fig. 4. The D_{junction} value of a touching vessel is plotted in Fig. 4(a), the higher D_{junction} value, the brighter voxels. In Fig. 4(b) and (c), the D_{junction} value is threshold using different T_2. It can be observed that most of the voxels removed by a relatively high threshold are from the connection region. That is, touching vessel is separated further with a higher T_2, while the shapes and positions of two vessels are retained. Therefore, to obtain a good separation, threshold

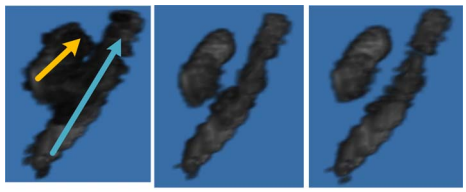

Fig. 4. Illustration of touching branches that are separated using D_{junction} and threshold. (a) D_{junction} of touching vessels, (b) $T_2 = 0.1$, (c) $T_2 = 0.15$.

T_2 is usually to be set of a relatively high value. The threshold 0.1 is sufficient for datasets we tested.

C. Grouping on Branch Level

Modern medical imaging modalities depict vessel systems of human body in details, and there is no ambiguity to identify arteries and veins [1]. Here, it is assumed that the topology of vasculatures is stable and a genuine connection can be found from a vessel branch to its vasculature in case that branch and vasculature are visually discontinuous on CT images.

After voxel-level grouping, a set of vessel branches or fragments is obtained. A branch-level grouping is then conducted globally, which groups vessel branches to connect one another into a vasculature. In liver vasculature segmentation, it starts from the two branches at the entries of the hepatic vein and portal vein in liver, which can be determined heuristically/manually. Let HV denotes the hepatic vein, which initially consists of one branch at the hepatic vein entry. Let PV denotes the portal vein, which initially consists of one branch at the portal vein entry. The algorithm extends HV and PV by adding in a new branch with a fit connection to them iteratively till HV grows into the full hepatic vein and PV grows into the full portal vein finally. The branches without fit connections to both veins are treated as nonvessel structures and are discarded. The priority of a branch to process is according to a key value $key_B = sqrt(N_B)/\max(D(\mathrm{B},\mathrm{HV})), D(\mathrm{B},\mathrm{PV}))$, where B is a candidate branch, HV is the hepatic vein, and PV is the portal vein. N_B is the number of voxels in B. $D(\mathrm{B},\mathrm{HV})$ is the minimum Euclidean distance between B and HV and is calculated as $D(\mathrm{B},\mathrm{HV}) = \min_{b\in B, hv\in \mathrm{HV}}(|\sqrt{(b_x - hv_x)^2 + (b_y - hv_y)^2 + (b_z - hv_z)^2}|)$. Similarly, $D(\mathrm{B},\mathrm{PV})$ is calculated. The processing priority prefers large branch and close distance, since large branch is relatively stable under noisy environment and the connection within a close distance is relatively robust to disturbance. To identify fit connections, a multiple feature point voting mechanism is employed.

1) Multiple feature point voting mechanism: In recent work [12], topological analysis of a branch with or without bifurcations is conducted before determining whether it has fit connections with vessel trees. Topology is analyzed based on central lines/skeletons, whose extraction needs lots of effort and is prone to error. To identify fit connections robustly, multiple feature point voting is proposed, which includes four steps.

First, the method extracts feature points on a vessel branch. The feature points are those possible points within neighborhoods of potential connection regions from branch to the trees. For example, given a branch, to classify it to HV or PV, four feature points are selected: 1) root1: the boundary point where the vessel is most salient; 2) root2: the central point where the vessel is the biggest; 3) connection point to HV: the nearest point to the hepatic vein; 4) connection point to PV: the nearest point to the portal vein. Ideally, root1, root2, and one of connection points to the vein should be the same one or very closed to one another since they correspond to the features of the same genuine connection point. Practically, they are different. The reason of using multiple feature points is to avoid the loss of these points within/nearby genuine connection regions by a single selection rule. More feature points can increase the robustness, but they increase the computational cost as well. One can choose more/less feature points to gain a balance in different applications and image qualities. The aforementioned four features are sufficient for our application.

Second, these feature points vote on optimal connections to the trees through *connectivity*s. One feature point has one optimal connection with one tree, which has maximal connectivity. The connectivity is calculated using (4), where $\sigma_1 = \max_{B_i,B_j\subset B}(D(B_i,B_j))$ and $\sigma_2 = 1/2\sigma_1$. B_i and B_j are two vessel branches, and $D(B_i, B_j)$ is the minimal Euclidean distance between B_i and B_j. The physical meaning of σ_1 is maximal distance among all vessel branches. The meaning of σ_2 is the curvature of a circle with σ_1 as diameter. σ_1 and σ_2 are set using one training volume and fixed for all experiments. To be robust to noise, the direction of feature point is recalculated within its neighborhood using principal component analysis (PCA) [20].

Third, the feature point having distinguishable connections with different vessel trees is recognized as unambiguous connection point. Here, connections are numerically distinguished by *connectivity*s. For example, give a set of feature points P, the unambiguous connection point p to HV and PV can be identified using

$$|\Delta C_p| = \max_{pt\in P}(|\text{connectivity}_{(pt,\mathrm{HV})} - \text{connectivity}_{(pt,\mathrm{PV})}|) \tag{9}$$

i.e., p is the feature point where the differences of *connectivity* is maximized.

Finally, the optimal connection from this unambiguous point is identified as a fit connection of the branch to the tree. The branch is accordingly classified as the tree on the other side of the fit connection. For an instance of the earlier unambiguous connection point p, whose branch B can be classified to HV or PV using

$$B \subset \begin{cases} \mathrm{HV}, & \text{if } \Delta C_p > 0 \\ \mathrm{PV}, & \text{if } \Delta C_p < 0 \end{cases}. \tag{10}$$

The proposed voting mechanism can be generalized to other applications. For applications having one vasculature, the connectivity to the second tree can simply be set as zero. For applications having three vasculatures, the feature points vote on three connections and select the optimal one.

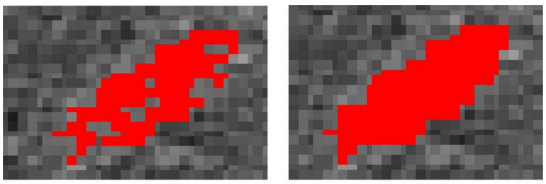

(a) (b)

Fig. 5. Example results: voxels detected as vessel are marked in red (a) before postprocessing, (b) after postprocessing.

D. Postprocessing

After hierarchical grouping, the postprocessing is conducted for vessel smoothing and hole-filling. A confidence connected component extension [21] followed by a morphological closing operation [22] is adopted for postprocessing. These are 2-D algorithms and process CT volumes slice by slice. The confidence connected component expands the vasculatures slightly and fills some holes/concaves. The morphological closing operation smoothes the vasculatures and fills the holes. An example result is displayed in Fig. 5. A slice of vessel branch with holes inside is shown in Fig. 5(a). After postprocessing, it become more smoothly and the holes are filled, as illustrated in Fig. 5(b).

III. Experimental Results and Discussion

The proposed method was evaluated on ten clinical CT scans at the portal venous phase. The data included liver CT from ten patients acquired on one 64-detector scanner (SOMATOM Sensation, Siemens Medical Solutions, Forchheim, Germany), using a standard four-phase contrast-enhanced imaging protocol with the slice thickness of 1.5–3.0 mm, matrix of 512 × 512 pixels, and in-plane resolution of 0.59–0.78 mm.

The voxel segmentation accuracy [23] is set as one of the performance measures. It is estimated by the ratio of the total number of correctly classified points (sum of true positives and true negatives by the number of points in the liver ROI). Other important measures are sensitivity and specificity, which are indicators of the number of properly classified pixels, respectively, in the true positive and true negative classes. The overlap measure is calculated as the ratio of the true positive to the sum of the true positive, the false positive, and the false negative by the number of points. The average distance between vessel boundaries and those of the ground truth is also calculated to measure the deviation of the misclassified vessel from the ground truth. In addition, the recognition rate at branch-level grouping is defined as the ratio of the number of properly/correctly classified branches, to either the portal vein or hepatic vein, to the total number of grouped branches of the two veins. The total number of grouped branches is n, if no more segmented branches can be grouped to veins after top n segmented branches were grouped. The ground truth employed was a segmentation result generated[1] by a medical imaging specialist with ten-year experiences using MIUE [17] and verified by a radiologist. For a typical CT volume with resolution 0.76 × 0.76 × 2.0 and dimension 512 × 512 × 112, the process time is about 3 min when running on a PC with CPU 2.0 GHz, 2.0 GB of RAM.

TABLE I.
Performance of the Proposed Method

CT Volume	Ac	Se	Sp	Om	Ad (mm)	Rr
CT_01 R:0.67×0.67×3.0 D:512×512×61	0.98	0.78	0.99	0.64	1.20	0.94
CT_02 R:0.59×0.59×3.0 D:512×512×83	0.98	0.71	0.98	0.56	1.25	0.99
CT_03 R:0.71×0.71×3.0 D:512×512×64	0.98	0.74	0.99	0.53	0.91	0.95
CT_04 R:0.67×0.67×3.0 D:512×512×55	0.96	0.56	0.98	0.41	4.45	0.99
CT_05 R:0.62×0.62×3.0 D:512×512×54	0.98	0.64	0.99	0.51	1.15	0.90
CT_06 R:0.61×0.61×3.0 D:512×512×44	0.97	0.72	0.98	0.51	2.60	0.99
CT_07 R:0.69×0.69×1.5 D:512×512×136	0.98	0.74	0.99	0.61	3.78	0.93
CT_08 R:0.69×0.69×1.5 D:512×512×160	0.97	0.59	0.99	0.49	4.23	0.98
CT_09 R:0.77×0.77×1.5 D:512×512×280	0.97	0.79	0.98	0.60	1.38	0.95
CT_10 R:0.78×0.78×2.0 D:112×512×112	0.98	0.72	0.99	0.62	1.90	0.96
average	0.98	0.70	0.99	0.55	2.28	0.96

Ac: accuracy, Se: sensitivity, Sp: specificity, Om: Overlap measure, Ad: average distance, Rr: recognition rate (branch level).

Table I illustrates the performance of proposed method. It can be observed the average segmentation accuracy is up to 98%. The highest sensitivity is 79% and the lowest is 56%. Similarly, the overlap measure is from 41% to 64%. The specificity is from 97% to 99%. The average segmentation accuracy and specificity are very high, while sensitivity is relatively not high. There is about 20% difference. The reason is that sensitivity only measures the segmentation accuracy of the vessels, the specificity only measures the segmentation accuracy of the nonvessels (the background and invisible vessels), and the average segmentation accuracy averages the accuracy of both vessels and nonvessels. Since visible vessels account for a small part of a liver volume, the number of properly classified nonvessels dominates the average segmentation accuracy. The earlier analysis indicates the proposed method is excellent at classifying vessels and nonvessels and promising in identifying all visible vessels. The average distance is from 0.9 to 4.4 mm. It indicates that the misclassified vessels do not deviate from the ground truth far away. In addition, the branch-level recognition rate is above 90%, which

[1]The ground truth was generated by a radiologist and a medical imaging specialist with ten year experiences. The medical imaging specialist generated an initial result by segmenting a CT volume using image processing techniques, e.g. thresholding. The radiologist compared the segmented result with the CT scan and gave the advices on how to improve the initial result. Accordingly, the medical imaging specialist revised it manually using image edit tools. The result was not revised until it was accepted by the radiologist. The finally verified result becomes the ground truth.

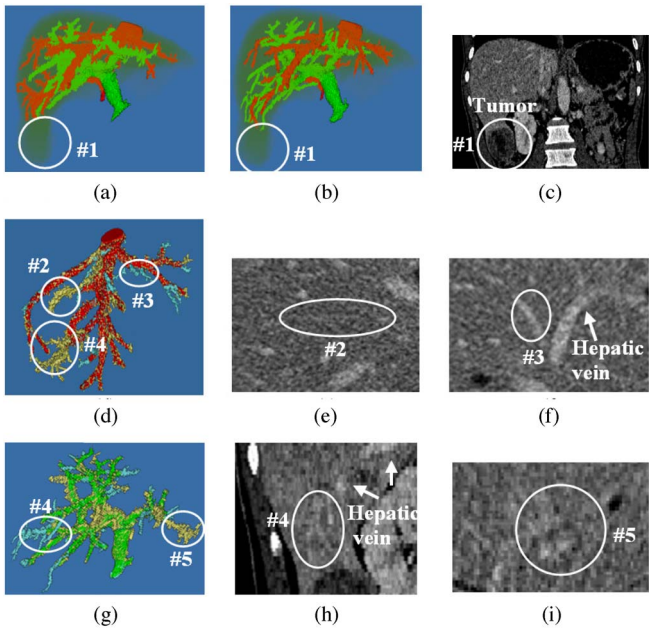

Fig. 6. Example results on liver vasculature little affected by tumors: (a) ground truth: hepatic (red) and portal vein (green); (b) segmented results: hepatic (red) and portal vein (green); (c) #1: vessels missing inside the tumor; (d) hepatic vein comparison of ground truth with segmented result (red: overlap vessels, yellow: undersegmented vessels, blue: oversegmented vessels.); (e) #2: an undersegmentation; (f) #3: an oversegmented vessel (it is actually a true vessel); (g) portal vein comparison of ground truth with segmented result (green: overlap vessels, yellow: undersegmented vessels, blue: oversegmented vessels); (h) #4: an oversegmentation (it is actually a misclassification branch); (i) #5: an undersegmentation.

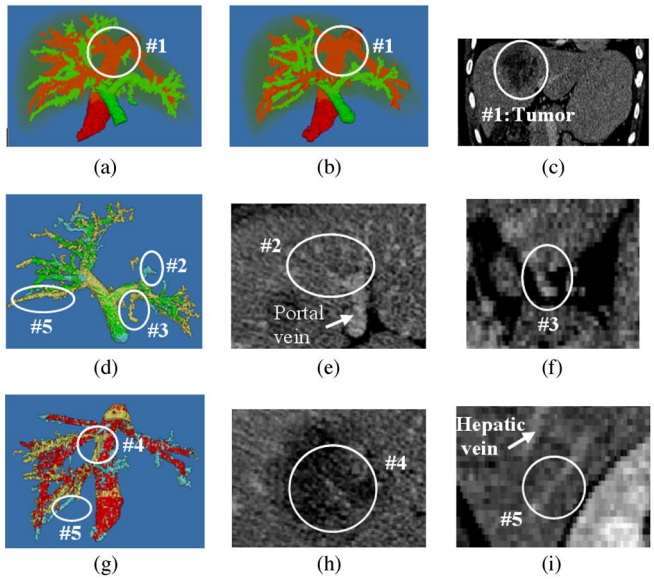

Fig. 7. Example results on liver vasculature seriously affected by tumors: (a) ground truth: hepatic (red) and portal vein (green); (b) segmented results: hepatic(red) and portal vein(green); (c) #1: vessels missing inside a tumor; (d) comparison of ground truth with segmented portal vein.(green: overlap vessels, yellow: undersegmented vessels, blue: oversegmented vessels.); (e) #2: oversegmented vessel (it is actually a true low-contrast vessel); (f) #3: undersegmentation (beyond liver ROI); (g) comparison of ground truth with segmented hepatic vein (red: overlap vessels, yellow: under segmented vessels, blue: oversegmented vessels.); (h) #4: undersegmentation inside tumor; (i) #5: misclassification of portal vein and hepatic vein.

indicates that most of grouped branched can be classified as the hepatic vein and portal vein correctly.

Two examples are used to visually illustrate the segmentation results and analyze the difference between ground truth and segmentation results. Fig. 6(a) displayed ground truth vasculatures of a liver volume with a peripheral liver tumor. Fig. 6(b) displayed segmented vasculatures. It can be observed that no vessel is detected in the tumor region, #1 region. The original tumor region is marked in Fig. 6(c) for clarity. Because the tumor is dark in CT image and its intensity is lower than the threshold of vessel intensity, the voxels inside may be treated as nonvessel in voxel-level grouping. A special mechanism is required to handle vessel inside the tumor, which will be our future work.

It is interesting that the expert observer also find it is difficult to label vessels inside the tumor. Fig. 6(d) displays comparison results of the ground truth hepatic vein and segmented hepatic vein. The overlap of ground truth and segmented results is in red. The oversegmentation, i.e., the vessels detected by the proposed method but not marked in the ground truth is in blue. The undersegmentation, i.e., the vessels marked in the ground truth but not detected by the proposed method is in yellow. It can be observed that most of segmentation differences are at the vessel surface and tip of vessel branches. An undersegmentation and an oversegmentation are marked as #2 and #3, respectively. The original slice is displayed in Fig. 6(e) and (f) for examination. With regard to under segmented vessel, #2, its contrast to the background is observed very low, as shown in Fig. 6(e). The low contrast may lead to detection failure. As for the oversegmented vessel, #3, it is not a segmentation error. It is actually a true vessel that the human observer overlooked, as can be observed in the CT slice in Fig. 6(f). Fig. 6(g) displays comparison results of the portal veins of ground truth and segmented result. The overlap is in green. The oversegmentation is in blue and the undersegmentation is in yellow. Similarly, most of segmentation differences are at the vessel surface and tip of vessel branches. An oversegmentation and an undersegmentation are marked as #4 and #5, respectively. The original slice is displayed in Fig. 6(h) and (i) for examination. With regard to oversegmentation, #4, it is a misclassified branch, which is recognized as the portal vein by the proposed method, as shown in Fig. 6(g), but it is actually the hepatic vein marked in the ground truth, as shown in Fig. 6(d). The reason for misclassification may be that the bifurcation of this branch from the hepatic vein is too noisy to observe, as shown in Fig. 6(h). Even though the proposed method misclassified this branch, it segmented the branch better than the ground truth, i.e., it did not include too much background voxels into the branch. Regarding the undersegmentation, #5, the tubular structure of the vessel is worsened by the noise, as shown in Fig. 6(i).

Fig. 7(a) displays ground truth vasculatures of a liver volume with tumor near inferior vena cava. Fig. 7(b) illustrates the segmented vasculatures. Similarly, no vessel is detected in the tumor region using our method. The original tumor region is marked in Fig. 7(c) for clarity. Fig. 7(d) displays the comparison results of the ground truth portal vein and segmented

portal vein. The overlap is in green. The oversegmentation is in blue and the undersegmentation is in yellow. It can also be observed that most of segmentation errors are at the vessel surface and tip of vessel branches. One oversegmented vessel and one undersegmented vessel are marked as #2 and #3, respectively. The original slice is displayed in Fig. 7(e) and (f) for examination. The oversegmentation, #2, is not a segmentation error. It is actually a true vessel detected by the proposed method but overlooked by the observer. This can be verified in Fig. 7(e), where it can be found this vessel is a low contrast branch of the portal vein. The undersegmentation, #3, did not detected by the proposed method. By examining the CT slice in Fig. 7(f), it was found that the undersegmentation is beyond the liver ROI. Due to the assumption in Section II, the voxels outside the liver ROI will not be processed. Fig. 7(g) displays the comparison results of the ground truth hepatic vein and segmented hepatic vein. The overlap is in red. The oversegmentation is in blue and the undersegmentation is in yellow. One undersegmentation and one oversegmentation are marked as #4 and #5, respectively. The CT scans are displayed in Fig. 7(h) and (i) for examination. The undersegmented vessel, #4, is found within a tumor, as displayed in Fig. 7(h). Because its intensity is lower than the threshold of vessel intensity, the voxels may be treated as nonvessel in voxel-level grouping. The oversegmentation, #5, is a misclassified branch. It is the portal vein in the ground truth, as shown in Fig. 7(d) and is misclassified as the hepatic vein by the proposed method as shown in Fig. 7(g). The branch-level recognition rate is listed in Table I. More than 90% branches can be classified correctly.

Generally, the segmentation differences between segmented result and ground truth are at the vessel surface and branch tip. Under segmented vessels are more than over segmented vessels since a low false positive rate is kept. Most of the oversegmentations are not segmentation errors but overlooked vessels by observers. Most of undersegmentations are segmentation errors, which occur under inverse environment, such as low contrast and noise. In addition, misclassification of the hepatic veins and portal vein can also generate segmentation errors.

Quantitative comparisons with competing methods [10]–[12], [14] are needed to justify the proposed method. However, a lack of public databases and public implementation of these methods make it infeasible currently. Here, we make an attempt to give a result comparison with the level set-based method [21], which had been adapted for cerebral vasculature [3] and coronary artery segmentation [24]. The segmentation result is obtained after 10 000 iterations and shown in Fig. 8(a). Several seed points are manually selected on the portal vein and hepatic vein. The level set-based method cannot differentiate the portal vein and hepatic vein. It stays on voxel level, and no branch-level performance can be measured. The proposed method has an average 96% branch-level recognition rate, as shown in Table I. Thus, quantitative comparison is inappropriate and a proper comparison study is awaited. Visually, result comparison with that generated by the proposed method on voxel level is shown in Fig. 8(b)–(d). It can be observed that most of the oversegmentations (the level set method marked as vessels while our method did not) are on the vasculature surface and most of the undersegmentations (our method marked as vessels while the level set method did not) are on the small vessels. Therefore, the proposed method is superior to the level set-based method on vein discrimination and small branch segmentation.

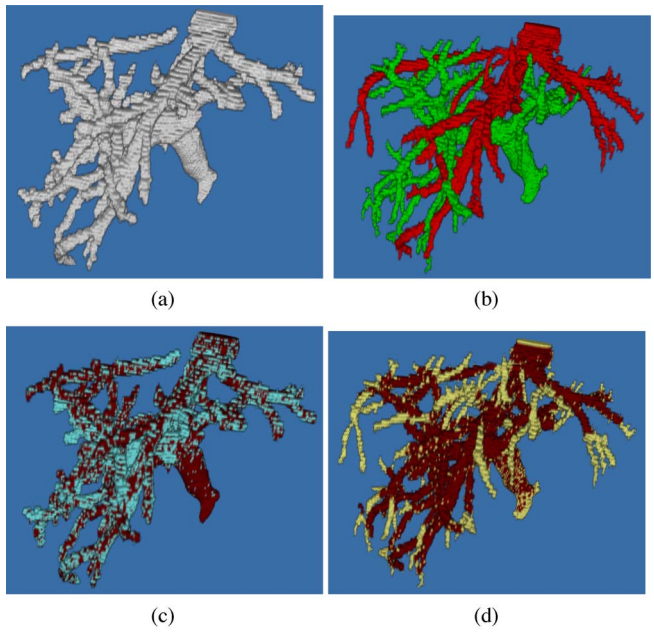

Fig. 8. Result comparison: (a) liver vasculature segmented using level set-based method [21]; (b) results using the proposed method. (c) Veins comparison the proposed method (red: overlap vessels, blue: oversegmented vessels; (d) veins comparison with the proposed method (red: overlap vessels, yellow: undersegmented vessels).

IV. Conclusion and Future Work

In this paper, a novel method is proposed for liver vasculature segmentation. It is able to segment and identify liver vasculatures from contrast enhanced CT images by using region-based features, which are simple but robust to noise and effective on distinguishing vessels. It extracts vasculature both locally and globally based on vessel context, which enables its coping with vasculatures of pathologic (tumor) volumes. It is computationally efficient by employing multiple feature point voting mechanism to classify vessel branches. It was tested on ten clinical CT datasets and results are promising. The third-order branches of vasculatures were segmented from the low resolution CT scans. In the future, we expect to improve the method by automating the threshold selection. Moreover, we will generalize the proposed method to high-resolution CT scans for fourth or higher order of vasculatures. In addition, we will improve the validation by analyzing vascular quantitatively and measuring inter/intraobservers' variations in ground truth. Also, vessel detection inside a tumor will be conducted to generalize the proposed method to other applications, e.g., angiogenesis monitoring. Finally, convincible/proper algorithm comparisons will be the aim for our future study.

REFERENCES

[1] K. Valji, *Vascular and Interventional Radiology*. vol. 10, Philadelphia, PA: W. B. Saunders Company, 1999, pp. 204–237.

[2] C. K. Wong and C. S. Chung, "Probabilistic vessel axis tracing and its application to vessel segmentation with stream surfaces and minimum cost paths," *Med. Image Anal*, vol. 11, pp. 567–587, 2007.

[3] R. Manniesing, B. K. Velthuis, M. S. Leeuwen, I. C. Schaaf, P. J. Laar, and W. J. Niessen, "Level set based cerebral vasculature segmentation and diameter quantification in CT angiography," *Med. Image Anal*, vol. 10, pp. 200–214, 2006.

[4] A. Gooya, L. Hongen, K. Matsumiya, K. Masamune, Y. Masutani, and T. Dohi, "A variational method for geometric regularization of vascular segmentation in medical images," *IEEE Trans. Image Process*, vol. 17, no. 8, pp. 1295–1312, Aug. 2008.

[5] C. Florin, N. Paragios, and J. Williams, "Particle filters, a quasi-Monte Carlo solution for segmentation of coronaries," in *Proc. Int. Conf. Med. Image Comput. Comput.-Assisted Intervention*, 2005, pp. 246–253.

[6] S. D. Olabarriaga, M. Breeuwer, and W. J. Niessen, "Minimum cost path algorithm for coronary artery central axis tracking in CT Images," in *Proc. Int. Conf. Med. Image Comput. Comput.-Assisted Intervention*, 2003, vol. 2879, pp. 687–694.

[7] P. H. Kitslaar, M. Frenay, E. Oost, J. Dijkstra, B. Stoe, and J. Reiber, "Connected component and morpholgy based extraction of arterial centerlines of the heart," in *Proc. Int. Conf. Med. Image Comput. Comput.-Assisted Intervention*, 2008.

[8] A. Szymczak, A. Stillman, A. Tannenbaum, and K. Mischaikow, "Coronary vessel trees from 3D imagery: A topological approach," *Med. Image Anal*, vol. 10, pp. 548–559, 2006.

[9] D. Lesage, E. D. Angelini, I. Bloch, and G. F. Lea, "A review of 3D vessel lumen segmentation techniques: Models, features and extraction schemes," *Med. Image Anal.*, vol. 13, pp. 819–845, 2009.

[10] O. Friman, M. Hindennach, C. Kuhnel, and H.-O. Peitgen, "Multiple hypothesis template tracking of small 3D vessel structures," *Med. Image Anal*, vol. 14, pp. 160–171, 2010.

[11] S. Esneault, C. Lafon, and J.-L. Dillenseger, "Liver vessels segmentation using a hybrid geometrical moments/graph cuts method," *IEEE Trans. Biomed. Eng.*, vol. 57, no. 2, pp. 276–283, Feb. 2010.

[12] C. Bauer, T. Pock, E. Sorantin, H. Bischof, and R. Beichel, "Segmentation of interwoven 3d tubular tree structures utilizing shape priors and graph cuts," *Med. Image Anal*, vol. 14, pp. 172–184, 2010.

[13] D. Shaked and A. M. Bruckstein, "Pruning medial axes," *Comput. Vis. Image Understanding*, vol. 69, pp. 156–169, 1998.

[14] O. C. Eidheim, L. Aurdal, T. O. Jensen, T. Mala, and B. Edwin, "Segmentation of liver vessels as seen in MR and CT images," *Int. J. Comput.-Assisted Radiol. Surg.*, vol. 1268, pp. 201–206, 2004.

[15] D. Selle, B. Preim, A. Schenk, and H.-O. Peitgen, "Analysis of vasculature for liver surgical planning," *IEEE Trans. Med. Imag*, vol. 21, no. 11, pp. 1344–1357, 2002.

[16] Y. Chi and M. K. H. Leung, "A general shape context framework for object identification," *Comput. Vis. Image Understanding*, vol. 12, pp. 324–336, 2008.

[17] http://www.liversuite.com, 2010.

[18] A. F. Frangi, W. J. Nissen, K. L. Vincken, and M. A. Viergever, "Multiscale vessel enhancement filtering," in *Proc. Int. Conf. Med. Image Comput. Comput.-Assisted Intervention*, 1998, pp. 130–137.

[19] G. Medioni, C. K. Tang, and M. S. Lee, "Tensor voting: Theory and applications," in *Proc. RFIA*, 2000.

[20] http://www.cs.otago.ac.nz/cosc453/student_tutorials/principal_components.pdf, 2002.

[21] T. S. Yoo, M. J. Ackerman, W. E. Lorensen, W. Schroeder, V. Chalana, S. Aylward, D. Metaxes, and R. Whitaker, "Engineering and algorithm design for an image processing API: A technical report on ITK - The Insight Toolkit," in *Proc. Medicine Meets Virtual Reality*, J. Westwood, ed., Amsterdam: IOS Press, 2002, pp. 586–592.

[22] J. Serra, *Image Analysis and Mathematical Morphology*. New York: Academic, 1982.

[23] A. M. Mendonca and A. Campilho, "Segmentation of retinal blood vessels by combining the detection of centerlines and morphological reconstruction," *IEEE Trans. Med. Imag.*, vol. 25, no. 9, pp. 1200–1213, Sep. 2006.

[24] L. Antiga, M. Piccinelli, L. Botti, B. Ene-Iordache, A. Remuzzi, and D.A. Steinman, "An image-based modeling framework for patient-specific computational hemodynamics," *Med. Biol. Eng. Comput.*, vol. 46, pp. 1097–1112, 2008.

Yanling Chi received the Ph.D. from the School of Computer Engineering, Nanyang Technological University (NTU), Nanyang, Singapore, in 2007.

She was with the National University of Singapore and NTU and joined Singapore Bioimaging Consortium in 2009. She is currently a Research Fellow at the Biomedical Imaging Laboratory, A∗STAR, Singapore. Her research interests include image processing, pattern recognition, and computer vision. She has experiences in content-based image retrieval, object recognition, health care/monitoring, robotics.

Jimin Liu received the Bachelor's degree in mathematics from the National University of Defense Technology, China, the Master's degree in mathematics from East China Normal University, Shanghai, China, and the Ph.D. degree in computer science from the Institute of Computing Technology, Chinese Academy of Science, Beijing, China, in 2000.

He is currently with the Biomedical Imaging Laboratory, A∗STAR, Singapore. His research interest include medical image processing, which also include segmentation, modeling, registration, and visualization.

Sudhakar K. Venkatesh received the MBBS degree from Bangalore University, Bangalore, India, in 1994, the M.D. degree from Delhi University, Delhi, India, in 1997, the DNB-Diplomate in National Board of Examinations-Radiodiagnosis, New Delhi, India, 1997, the FRCR-Fellow in Royal College of Radiologists, London, U.K., in 2003, and the MMed degree in Diagnostic Radiology from the National University of Singapore, Singapore, in 2003.

He is currently an Assistant Professor of diagnostic radiology, Department of Diagnostic Imaging, National University Hospital, Singapore (NUHS), where he is also a Consultant in Diagnostic Imaging. He is an expert Abdominal Radiologist and Interventional Radiologist. He recently received a special training in MRE of liver at Mayo Clinic, Rochester, MN. He has been instrumental in bringing the MRE technique to NUH and he is currently doing many projects on MRE of liver at NUH. He is the author or coauthor of more than 40 peer-reviewed articles published in international journals. He is engaged in research on general procedures, such as biopsy, drainages, and vascular access. His special interest is in locoregional treatment of liver tumors, including yttrium-90 radio ablation and chemoembolization of tumors.

Dr. Venkatesh is a recipient of many international and regional awards. He also holds several grants including National Medical Research Council, Individual Research Grant for Magnetic Resonance Elastography (MRE) of liver and is a collaborator of many research projects.

Su Huang received the B.Sc. degree in computational mathematics from Zhongshan University, Guangzhou, China, in 1982, and the M.Sc. degree in computer science from Peking University, Beijing, China, in 1989, respectively.

He is currently with the Biomedical Imaging Laboratory, A∗STAR, Singapore. He has been involved in medical image research since 1998, and he is currently a Research Project Manager in Singapore Bioimaging Consortium. His research interests include medical image analysis and visualization innovative algorithms investigation and tools development.

Jiayin Zhou (S'01–M'06) received the Bachelor's and Master's degrees in biomedical engineering from Zhejiang University, Zhejiang, China in 1997 and 2000, respectively, and the Ph.D. degree from Nanyang Technological University (NTU), Singapore, in 2005.

From 2004 to 2009, he was with NTU and then in the National University of Singapore as a Researcher for several medical image processing and analysis projects. Since 2009, he has been with the Institute for Infocomm Research, A∗STAR, Singapore. His current research interests include medical image processing and analysis, computer-aided diagnosis, and quantitative imaging metrics.

Dr. Zhou is a member of the Engineering in Medicine and Biology Society.

Qi Tian (S'83–M'86–SM'90) received the B.S. and M.S. degrees from the Tsinghua University, Beijing, China, and the Ph.D. degree from the University of South Carolina, Columbia, respectively, all in electrical and computer engineering.

He is currently a Principal Scientist at the Institute for Infocomm Research, A∗STAR, Singapore. In 1992, he joined the Institute of System Science, National University of Singapore, as a Research Staff. He is the author or coauthor of more than 160 papers published in peer-reviewed international journals and conferences. His main research interests include image/video/audio analysis, multimedia content indexing and retrieval, medical image analysis, computer vision, statistical learning.

Dr. Tian has served as an Associate Editor for the IEEE TRANSACTIONS ON CIRCUITS AND SYSTEMS FOR VIDEO TECHNOLOGY from 1997 to 2004.

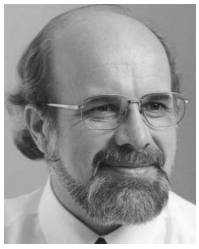

Wiesław L. Nowinski received the D.Sc. degree from Polish Academy of Sciences, Poland and the Ph.D. degree from Lodz Technological University, Poland.

He is currently a Principal Scientist and the Director of the Biomedical Imaging Laboratory, A∗STAR, Singapore. He is also an Affiliate Professor of radiology at the University of Washington Medical Center, Seattle, a Visiting Professor and Doctoral Advisor at Harbin Institute of Technology, China, and an Adjunct Professor at Nanyang Technological University, Singapore. He is the author or coauthor of more than published 473 papers, filed 50 patent applications (24 are already granted), and developed with his team 23 brain atlas products used worldwide in neurosurgery, neuroradiology, neurology, brain mapping, and neuroeducation. These atlases are incorporated in more than 1000 neurosurgical workstations (distributed by Medtronic, BrainLab, Elekta and other companies) as well as distributed on 7 CD-ROMs by Thieme Publishers to more than 5000 clinicians and medical schools. His research interests include brain atlases, stroke, deep brain stimulation, neuroinformatics, medical image processing, virtual reality, computer-assisted diagnosis and treatment, and future directions in computer-aided radiology and surgery.

Dr. Nowinski has been conferred with 33 awards and honors, including the *Magna cum Laude* (radiological Oscar) from the Radiological Society of North America in 2009, 2004, the European Congress of Radiology in 2000, the *Summa cum Laude* in 2008 and 1997, the *Magna cum Laude* in 2009 and 2005 from the American Society of Neuroradiology, and the *Knight's Cross of Merit* from the President of Republic of Poland in 2005.